Collapse of DNA in ac Electric Fields

Chunda Zhou,[1] Walter W. Reisner,[2] Rory J. Staunton,[1] Amir Ashan,[3] Robert H. Austin,[4] and Robert Riehn[1,*]

[1]North Carolina State University, Department of Physics, Raleigh, North Carolina 27695, USA
[2]McGill University, Department of Physics, Montréal, Quebec, Canada H3A 2T8
[3]Department of Physics, UCLA, Box 951547, Los Angeles, California 90095, USA
[4]Princeton University, Department of Physics, Princeton, New Jersey 08544, USA

(Received 30 January 2011; published 16 June 2011)

We report that double-stranded DNA collapses in the presence of ac electric fields at frequencies of a few hundred Hertz, and does not stretch as commonly assumed. In particular, we show that confinement-stretched DNA can collapse to about one quarter of its equilibrium length. We propose that this effect is based on finite relaxation times of the counterion cloud, and the subsequent partitioning of the molecule into mutually attractive units. We discuss alternative models of those attractive units.

DOI: 10.1103/PhysRevLett.106.248103 PACS numbers: 87.14.gk, 36.20.Ey, 82.35.Lr, 82.35.Rs

The mechanical response of DNA to alternating electric fields has been studied extensively with the consensus finding that molecules stretch along the direction of the field, as long as the field is spatially homogeneous. This effect was attributed to the global polarizability of a coil at low frequencies [1,2], and the high local anisotropy of the counterion transport at high frequencies [3,4]. Here we show that the behavior is drastically different at frequencies at which the counterion relaxation length scale matches the scale of internal density fluctuations. In particular, we show that a frequency range exists in which DNA collapses both from a quasifree coil configuration, and when prestretched through mechanical confinement. We link the observed collapse to the length-scale dependent polarizability of the coil, which partitions the molecule into subunits that interact as if they were independent coils [5,6].

Our finding presents a considerable challenge to models of polyelectrolyte electrodiffusion. In particular, our experiments critically probe the assumptions about the coupling of condensed counterions, free ions, and hydrodynamics [7–9]. It is not clear to which extent linearization and preaveraging of terms are applicable to our system. Numerical models are challenged by the large size of our system, and have only recently become treatable [10].

All experiments used micro- and nanofluidic devices made from fused silica, which were prepared by methods discussed elsewhere [11]. λ-DNA (48.5 kbp, contour length ≈ 16 μm) was suspended in 0.5 x TBE buffer and stained using an intercalating dye (YOYO-1) at the ratio of 1 dye per 10 base pairs. The mechanical [12] and electrophoretic parameters [13] are somewhat modulated by the staining (order or 10%), but DNA retains its essential characteristics. 0.1% by weight polydimethylacrylamide (POP, Applied Biosystems), which adsorbs onto channel walls, was added to prevent electroendosmosis [14]. The local DNA density was determined from the dye fluorescence intensity collected by an EM-CCD camera on a microscope with a resolution close to the diffraction limit. We used 10 ms exposure time at 10 Hz frame rate. We used two device layouts: a purely microfluidic layout with a 0.6×10 μm^2 channel cross section, and a mixed nano- or microfluidic layout with 80×100 nm^2 or 225×325 nm^2 nanochannel cross sections (Fig. 1). All micro- and nanochannels are hundreds of microns long. Voltages were applied using platinum wires. In nanochannel devices the field was controlled by placing the nanochannel between two microchannels that carried identical currents, but that were held at the desired potential difference [15]. We did not correct for concentration polarization at nanochannel or microchannel junctions. In microfluidic devices, the applied voltages were large enough to make the voltage drop at the electrodes small compared to the applied voltage. During application of the ac voltage, an additional small dc bias was applied if asymmetries between the electrodes gave rise to a net drift.

For microchannel devices with a depth comparable to the radius of gyration of DNA, Bonthuis *et al.* found only minor alterations of the configuration and dynamics of DNA when compared to the bulk [16]. DNA can assume an essentially undisturbed configuration in the lateral dimension [17]. Channels deeper than 600 nm were not explored because of the limited depth of field of the microscope objective. In nanochannels, DNA is mechanically

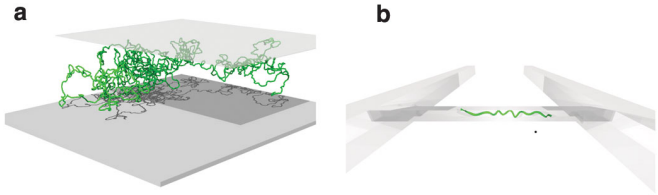

FIG. 1 (color). Schematics of device structures. (a) Microfluidic device with molecule of actual size. (b) Nanofluidic device with schematic molecule in nanochannel (center) bridging two microchannels (left and right).

stretched in an equilibrium process balancing entropic spring forces and self-avoidance [18]. Fitting the convolution of a boxcar function and a Gaussian to the intensity along the channel yields the molecule extension. The equilibrium extension along the channel length is in the range of 60% to 70% of the contour length for 80×100 nm^2 channels and ~20% for 225×325 nm^2 channels, respectively.

Figures 2(a)–2(c) show nanochannel-stretched molecules at increasing electric fields and a frequency of 300 Hz. We observe that below a threshold field strength, DNA is essentially unperturbed in its extended equilibrium configuration, while it collapses to about 20% of its equilibrium extension at high field strengths. The collapse is fast, and the lateral displacement is due to asymmetry of injecting electrodes during the first cycles. The fractional extension (ratio of end-to-end lengths with and without ac field) vs field amplitude graph for nanochannel confined DNA bears the signature of a phase transition, with a statistically significant noise maximum about half way through the transition (Fig. 3). A similar collapse in microchannels is shown in Figs. 2(d) and 2(e), where we present typical movie frames without and with an ac field applied, respectively. Critical fields for collapse were comparable in micro- and nanochannels.

We were able to replicate the collapse of microconfined DNA in 0.25 x to 2 x TBE buffers, with and without agents to suppress electroendosmosis. This suggests a low influence of electrohydrodynamic interactions between wall and polymer. Since the measurements under nanoconfinement suggest that long-range hydrodynamic coupling within the polymer is not leading either, it appears that hydrodynamic coupling overall plays a secondary role in the collapse.

A key insight into the collapse process is obtained by varying the frequency of the electric field (Fig. 4). We observed that the field strength needed for collapse rises with an increase in the drive frequency. Lower nanochannel width also raises the critical field strength for collapse. We can reasonably assume that this frequency dependence is caused by counterions relaxation dynamics [19], and further hypothesize that the dependence arises because the period of oscillation coincides with an intrinsic relaxation time. Using a single diffusive relaxation time τ for Tris H^+ ions, we can calculate that the polarization scale $\lambda_\omega = \sqrt{D/\omega}$, where D is the diffusion coefficient determined from the mobility data of Klein and Bates [20]. For a transition occurring at 500 Hz, λ_ω is about half a micron. That is beyond the effective diameter of DNA under our buffer conditions (a few nm), but much shorter than the stretched molecule. Comparing λ_ω to length-scales of the system, we notice that the length of a hairpin bend of DNA, the size of blobs in the de Gennes model, the persistence length, or the length of more general density fluctuations may fall into this length scale. The collapse of unconfined molecules provides an upper limit of the scale in the form of the mean radius of gyration of the molecule, about 700 to 800 nm. We postulate two distinct physical mechanisms that could lead to a contraction: mutual attraction of hairpins and mutual attraction of density fluctuations (Fig. 5). While both lead to qualitatively correct conclusions, we were unable to provide a quantitative comparison.

The mutual attraction of hairpins in our model is based on the frequency-dependent polarization of curved segments [21]. The model postulates that Manning-condensed counterions, which surround the molecule, only move along the backbone of the molecule. In a simplified model without thermal charge fluctuations the charge per unit length can be separated into a polarization charge density $\rho_p(s, t)$ and the average counterion charge per unit length ρ_0 which is of the order of e/b, with s the location along

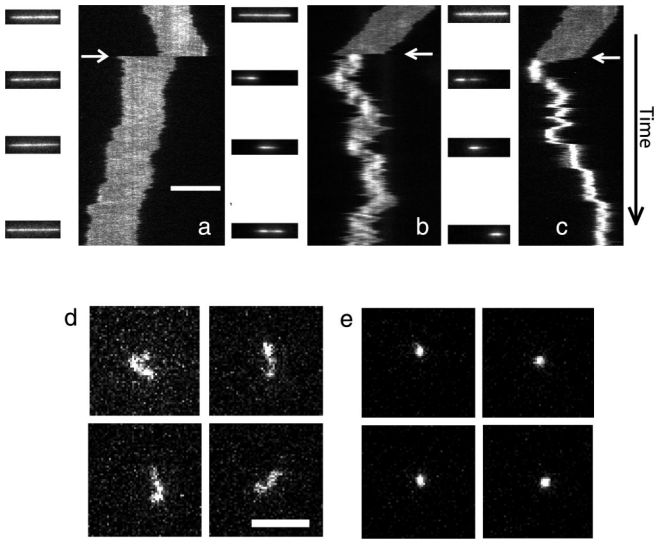

FIG. 2. Collapse of DNA in an ac electric field at 300 Hz. (a)–(c) Time traces of intensity along nanochannel-stretched DNA vs time ((A) 210 V/cm, (b) 420 V/cm, (c) 780 V/cm). Each line is a instantaneous intensity along the nanochannel axis, which have a cross-section of 80×100 nm^2. The small panels are individual movie frames. The horizontal scale is 10 μm, and the total time is 50 sec. The ac field was applied at the arrow. (d) and (e) Molecules in microchannel without and with electric field of 700 V/cm, respectively. Scale bar 5 μm.

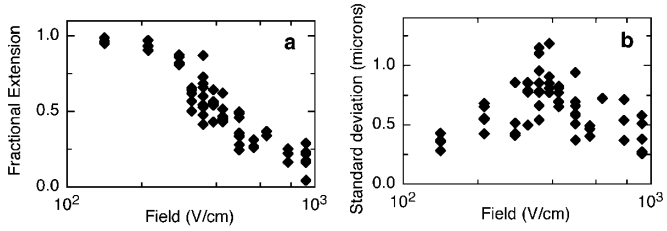

FIG. 3. (a) Fractional length vs field strength in 80×100 nm^2 nanochannels. Data shows spread of individual points. (b) Standard deviation within individual single-molecule traces.

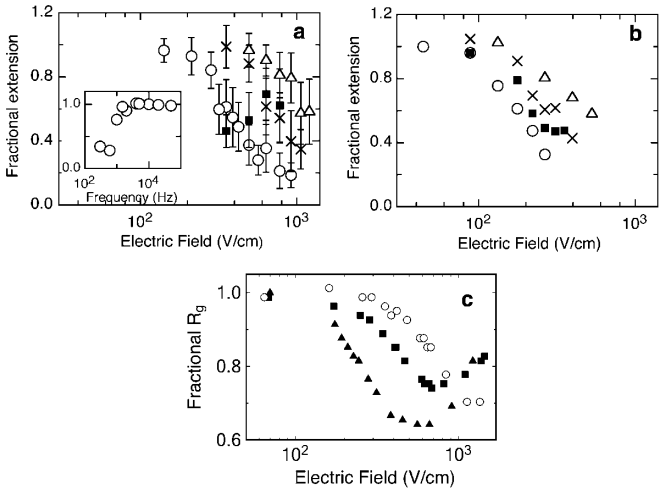

FIG. 4. Influence of frequency on contraction. (A) Fractional extension in 80 nm × 100 nm channels. Symbols: 100 (■), 300 (○), 500 (×), and 700 Hz (△). The inset show the contraction at 1.4 kV/cm over a large range of frequencies. Error bars are standard deviations of means. (B) Fractional extension in 225 nm × 325 nm channels. 300 (○), 400 (■), 500 (×), and 600 Hz (△). (C) Fractional radius of gyration (ratio of $\boldsymbol{Rg}$ to equilibrium $\boldsymbol{Rg}$) in microfluidic channels. 100 (▲), 300 (■), and 675 Hz (○).

the molecule, t the time, and b the base-pair spacing. The configuration of the molecule is characterized by the position $\vec{r}(s, t)$ and the tangent vector $\hat{t} = \partial\vec{r}/\partial s$. The polarization charge density $\rho_p(\omega, s)$ for a fixed molecule configuration can be computed from time Fourier transform of the linearized Nernst-Planck equation

$$i\omega\rho_p(\omega, s) \approx D\left(\frac{\partial^2\rho_p(\omega, s)}{\partial s^2} - \frac{\rho_0 e\vec{E}_\omega}{k_B T}\cdot\frac{\partial\hat{t}(s)}{\partial s}\right). \quad (1)$$

For high frequencies ($l_p < \lambda_\omega \ll \ell$), the average polarization of a stretched molecule is small, but a local charge density proportional to the dot product of curvature vector (averaged over λ_ω) and a local electric field is induced. Segments of opposing curvature carry opposite charge, and give rise to a mutual "polarization attraction." Collapse is expected when the attraction between hairpins exceeds the electrostatic repulsion. $\rho_p(\omega, s)$ must then exceed the net charge per unit length e/l_b of DNA under Manning condensation ($l_B \approx 1$ nm Bjerrum length). This leads to an upper limit for the bending radius of

$$r < \frac{l_b}{b}\frac{DeE_\omega}{\omega k_B T}. \quad (2)$$

For E_ω of 10^3 V/cm, and $1/b \approx 10^{10}$/m, the limiting radius is about 1 μm, clearly larger than the lateral nanochannel dimension and the persistence length. Hence, all full hairpins in nanochannels would be attracting. Beyond the strength of the interaction, a sufficient number of interacting segments within the molecule must approach close enough to experience the interaction. While there is

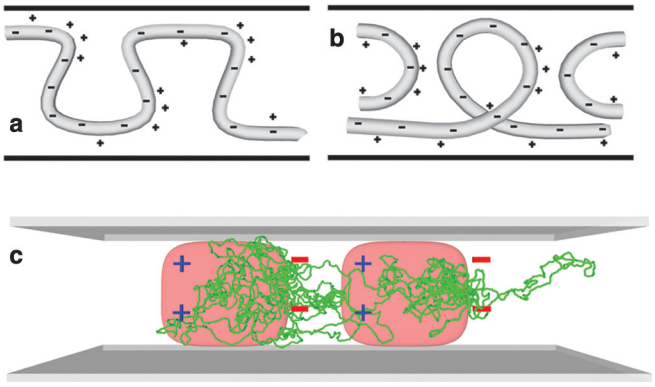

FIG. 5 (color). Model of collapses. (a) and (b) limiting geometries for "curvature condensation." The electric field polarizes only highly curved DNA segment, which then interact. (c) Polarization of density fluctuations. The counterion (pink) and coion (not shown) clouds are displaced to yield a local polarization that is polyelectrolyte density dependent, thus leading to local, interacting charges.

currently no broad consensus on the precise nature of the nanochannel stretching, we note that the stretching must be the result of interactions of chain segments along the molecule. The linearity of stretching at lengths beyond at least 1 μm in occupied channel length indicates that stretched molecules at least experience tens of interaction points. This is a lower bound on the number of contacts if we accept a self-avoidance based model [22,23]. For molecules confined in microchannels, the self-interaction probability for λ-DNA is low enough for the molecule to be Gaussian [17]. However, a disturbed counterion atmosphere is considerably larger than the one in equilibrium, and hence the induced interaction energy can exceed $k_B T$ between segments that would be too far apart to interact without a field.

The main criticism of the "curvature condensation" model is that the high electric fields applied here make a linear response, and polarization solely along the backbone of the polyelectrolyte, somewhat unlikely. Counterion dissociation [24], concentration polarization [25,26], or electrohydrodynamic [27,28] effects should be considered. Isambert *et al.* have developed a model for the aggregation and dynamics of a solution of polymer under ac electric fields that considers the depletion of co- and counterions as the *leading* effect, with a subsequent polarization of the ionic atmosphere [28]. We propose that their model should not only be applicable to the interaction between polymer coils, but also between density fluctuations of the same molecule.

A qualitative agreement between this concentration polarization model and our experiment is obtained from Isambert's approach that uses the k-space Fourier transform of the density fluctuations, where k is the wave vector. In an ac field only DNA density fluctuation modes with $k^{-1} < \lambda_w$ are polarized and interact (Fig. 5). A rising frequency thus reduces the number of possible interacting

fluctuations, which should lead to a rise in the field strength required for collapse. Further, since the equilibrium fluctuation displacement amplitude scales with k^{-1}, the longest and slowest active mode carries the leading contribution to the polarization interaction. The observation of earlier collapse in wider channels also follows because DNA in wider channels has a higher fluctuation amplitude for a given k vector. The main shortcoming of the model, as Isambert emphasizes, is that the collapse instability does not follow from linear analysis, and thus relies on numerical treatment.

We have tested the concentration polarization hypothesis by treating a nanochannel-stretched molecule using a one-dimensional numerical model that links a Brownian dynamics treatment of the polymer chain with a conventional electrodiffusion model for the counter- and coions, details of which we will publish later. Long-range hydrodynamic interactions were excluded because of the assumed efficient hydrodynamic screening. Local interactions were excluded because they are strongly dependent on the local structure, and thus cannot be treated by a coarse-grained model. The model leads to concentration polarization within the macromolecule, and the resulting force nucleates regions of high density.

Finally, we consider whether the collapse could be an artifact of our micro- and nanofluidic techniques. The leading cause would be variations in channel width and resulting dielectrophoretic polymer aggregation at points of high electric fields [11,29]. That appears unlikely since we observed movement of condensed regions along the channel. A second criticism is the neglect of ions in the Debye layer belonging to channel walls, which could lead to localized high electric fields and dielectrophoretic condensation on rough walls [30]. We estimate a sidewall roughness of less than 5 nm, comparable to the Debye layer thickness. The Debye layer thus provides efficient screening. Note that previously unexplained features in electrodeless dielectrophoresis seem to be described by the condensation mechanism proposed here in conjunction with induced surface charge densities at micro-sized features [29].

An artifact that limits the observable contraction is the center of mass motion of DNA molecules during an exposure period. It leads to an apparent elongation of molecules in the direction of the electric field. The magnitude of this motion is proportional to the electric field strength and the period of oscillation, and has more relative importance for molecules with smaller dimensions. We believe that the high-field shoulder in Fig. 4(c) and the functional dependence of the 100-Hz curve in Fig. 4(a) are due to this effect.

We thank Robijn Bruinsma for discussions. We acknowledge support from the National Institutes of Health (R21HG004383, R21CA132075). Part of this work was performed in part at CNF, supported by NSF (ECS-0335765).

*rriehn@ncsu.edu

[1] M. Jonsson, U. Jacobsson, M. Takahashit, and B. Norden, J. Chem. Soc., Faraday Trans. **89**, 2791 (1993).
[2] F. Oosawa, *Polyelectrolytes* (Marcel Dekker, New York, 1971).
[3] C. Walti, P. Tosch, A. G. Davies, W. A. Germishuizen, and C. F. Kaminski, Appl. Phys. Lett. **88**, 153901 (2006).
[4] A. E. Cohen, Phys. Rev. Lett. **91**, 235506 (2003).
[5] L. Mitnik, C. Heller, J. Prost, and J. L. Viovy, Science **267**, 219 (1995).
[6] H. Isambert, A. Ajdari, J.-L. Viovy, and J. Prost, Phys. Rev. Lett. **78**, 971 (1997).
[7] J. L. Barrat and F. Joanny, Adv. Chem. Phys. **94**, 1 (1996).
[8] U. Mohanty and N. C. Stellwagen, Biopolymers **49**, 209 (1999).
[9] S. A. Allison and D. Stigter, Biophys. J. **78**, 121 (2000).
[10] K. Grass, U. Böhme, U. Scheler, H. Cottet, and C. Holm, Phys. Rev. Lett. **100**, 096104 (2008).
[11] R. Riehn, R. H. Austin, and J. C. Sturm, Nano Lett. **6**, 1973 (2006).
[12] T. T. Perkins, D. E. Smith, R. G. Larson, and S. Chu, Science **268**, 83 (1995).
[13] C. Carlsson and M. Jonsson, Electrophoresis **17**, 642 (1996).
[14] R. S. Madabhushi, Electrophoresis **19**, 224 (1998).
[15] R. Riehn, M. Lu, Y. Wang, S. Lim, E. Cox, and R. Austin, Proc. Natl. Acad. Sci. U.S.A. **102**, 10 012 (2005).
[16] D. J. Bonthuis, C. Meyer, D. Stein, and C. Dekker, Phys. Rev. Lett. **101**, 108303 (2008).
[17] A. E. Cohen and W. E. Moerner, Proc. Natl. Acad. Sci. U.S.A. **104**, 12 622 (2007).
[18] J. Tegenfeldt, C. Prinz, H. Cao, S. Chou, W. Reisner, R. Riehn, Y. Wang, E. Cox, J. Sturm, and P. Silberzan *et al.*, Proc. Natl. Acad. Sci. U.S.A. **101**, 10 979 (2004).
[19] M. Mandel, Mol. Phys. **4**, 489 (1961).
[20] S. D. Klein and R. G. Bates, J. Solution Chem. **9**, 289 (1980).
[21] R. F. Bruinsma and R. Riehn, Chem. Phys. Chem. **10**, 2871 (2009).
[22] P. de Gennes, *Scaling Concepts in Polymer Physics* (Cornell University Press, Ithaca, NY, 1979).
[23] W. Reisner, J. P. Beech, N. B. Larsen, H. Flyvbjerg, A. Kristensen, and J. O. Tegenfeldt, Phys. Rev. Lett. **99**, 058302 (2007).
[24] G. S. Mannning, Biophys. Chem. **7**, 189 (1977).
[25] A. Cebers and I. Rubinstein, Int. J. Mod. Phys. B **16**, 2334 (2002).
[26] M. Fixman and S. Jagannathan, Macromolecules **16**, 685 (1983).
[27] S.-R. Yeh, M. Seul, and B. I. Shraiman, Nature (London) **386**, 57 (1997).
[28] H. Isambert, A. Ajdari, J.-L. Viovy, and J. Prost, Phys. Rev. E **56**, 5688 (1997).
[29] C. F. Chou, J. O. Tegenfeldt, O. Bakajin, S. S. Chan, E. C. Cox, N. Darnton, T. Duke, and R. H. Austin, Biophys. J. **83**, 2170 (2002).
[30] S. K. Thamida and H. C. Chang, Phys. Fluids **14**, 4315 (2002).